INVESTIGATION OF THE MELTING PROCESS OF BCC IRON USING DIFFERENT INTERATOMIC POTENTIALS

Sedat Sengul[1], Unal Domekeli[1], Murat Celtek[2]

[1]*Dept. of Physics, Trakya University, 22030, Edirne – TURKEY*
[2]*Faculty of Education, Trakya University, 22030, Edirne – TURKEY*

Abstract

In our study, we focused on the melting process of bcc iron element. In order to follow this process, Finnis Sinclair (FS), embedded atom method (EAM) and tight-binding (TB) many-body potentials, which were widely used in the literature, was preferred. Classical molecular dynamics (MD) simulations were performed with DLPOLY 2.0 open-source code. Volume-temperature, energy-temperature, pair distribution function (g(r)) and pair analysis method were used to explain the changes in the structure of bcc iron during the heating process. It was observed that all three potentials correctly predicted their physical properties such as lattice parameter and cohesive energy. Compared to others, there appears to be a good agreement between the liquid g(r) curve obtained from the TB potential and the experimental result reported in the literature. However, during the heating process, it was observed that while the EAM and Tersoff potentials yield the properties of bcc iron reliably, the TB potential could not predict the structure of bcc iron at low temperatures and the system was subjected to a solid-solid phase transition at higher temperatures. We believe that the results of this study will provide helpful information on which potential can more accurately explain the interactions between iron atoms in MD simulations.

Keywords: Iron, Finnis Sinclair potential, Tight-binding potential, Embedded atom method, Pair analysis.

INTRODUCTION

Today, as a result of scientific and technological developments, there have been great advances in the field of computational science, both in terms of software and source and hardware. Thanks to these positive developments, many theoretical kinds of research that have been difficult to experimentally and not fully understood for several decades have been opened to work with simulations in a computer environment, and calculation methods based on computer simulations have been developed [1–3]. One of the most important points of computer simulation techniques is to describe the interactions of each particle with another at the atomic level. A good representation of the behavior of the system in terms of interaction potential ensures that the data obtained from the molecular dynamics (MD) simulations are in agreement with the experimental results [4]. Many simulation methods, from quasi-experimental to quantum mechanical computation, have been developed to mimic the behavior of atoms in the scientific world. Among them, especially the MD simulations leading experimental studies in examining the thermodynamic and structural properties of a material are one of the most used methods. We used DLPOLY 2.0 open source software as the classic MD simulation package [5]. In our study, we focused on MD simulations of the element iron (Fe), which is widely used in all areas of technology. Some of the reasons why Fe is preferred are as follows; It has a lower price compared to other metals and has high strength. In addition, the automotive industry, ship hull construction, and building construction are among the areas where Fe is used the most. Since it is of great importance to understand the mechanism and kinetics of the solid-solid phase transition observed in the heating process in Fe, scientists have conducted many experimental and atomic simulation studies on it [6–9]. The melting process of bcc Fe has been studied in detail by using FS [10], EAM [11] and TB [12]

potentials, which are popular in the literature, since it is of great importance to accurately describe the interactions between atoms in the system in MD simulations.

EXPOSITION

Since the theoretical knowledge and parameters of the three different potentials we used will take up a lot of space, they are not included here. Readers can find detailed information about these potentials from the relevant sources for FS [10], EAM [2, 11, 13, 14] and TB [12, 15–18]. The cubic simulation box contains 6750 Fe atoms conforming to the bcc crystal lattice and periodic boundary conditions are applied to the x-, y- and z-directions of the box. Temperature and pressure were kept under control with the Berendsen thermostat and barostat and the MD simulation timestep was set to 1 fs. The heating rate is chosen as 10 K/ps. The system was heated at 50 K intervals from 0 K to 2500 K to obtain the liquid phase under an NPT ensemble. The EAM, FS and TB potentials estimate the lattice parameter ($a^{exp} = 2.870$ Å) and cohesive energy ($E_{coh}^{exp} = -4.280$ eV/atom) values of bcc Fe as $a^{EAM} = 2.875$ Å, $a^{FS} = 2.872$ Å and $a^{TB} = 2.859$ Å, $E_{coh}^{EAM} = -4.290$ eV/atom, $E_{coh}^{FS} = -4.280$ eV/atom and $E_{coh}^{TB} = -4.228$ eV/atom, respectively. Although the results seem close to each other, the results of the EAM and FS potentials show better agreement with the experimental results compared to the TB potential results. Volume-temperature (V-T) and energy-temperature (E-T) curves obtained using all three potentials during the heating process are shown in Figure 1(a) and (b), respectively. The first thing that stands out here is that all three potentials predict the melting point of bcc Fe at different temperatures. The melting points determined from the EAM-, FS-, and TB-MD simulations are 2300 K, 1950 K, and 1750 K, respectively, which deviate from the experimental value ($T_m^{exp} = 1811$ K) by 27.00%, 7.68%, and -3.37%, respectively. These results indicate that the TB and FS potentials predict the melting point of Fe more closely to the experiment than the EAM potential. The second striking thing is that while the V-T (for low temperatures only) and E-T (up to near melting points) values obtained from the EAM and FS potentials are very close to each other, the results of TB potential differ from them. Another interesting observation is that there is a slight deviation around the melting point in both curves obtained from the TB potential. It is difficult to get information from these graphs as to whether this is a statistical error or a sign of a solid-solid phase transition, but this point will be addressed later by interpreting the different analysis results.

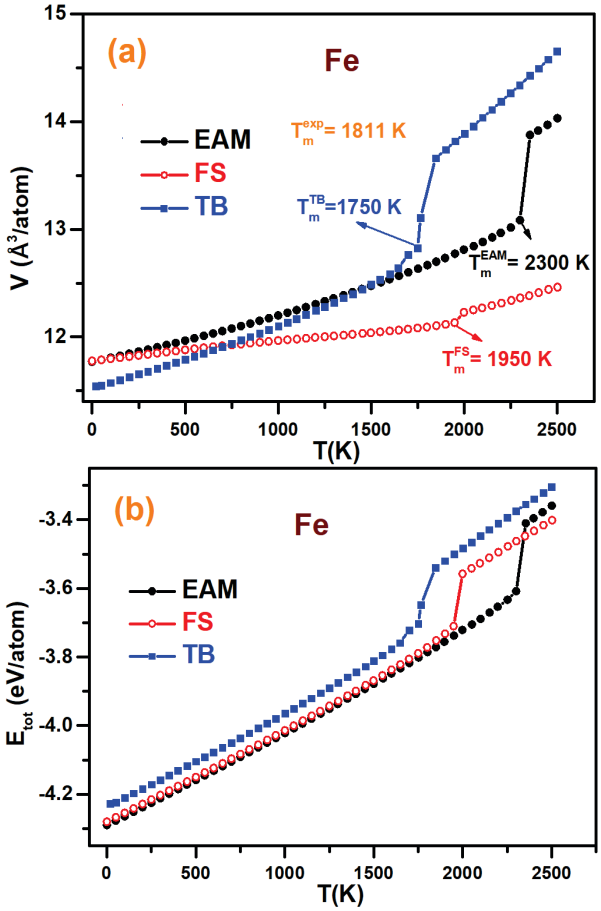

Fig. 1. *Variation of (a)V and (b) E values obtained from EAM, FS and TB potentials as a function of temperature during the heating process.*

How atoms are arranged in space, that is, their atomic-scale structure, is characteristic of the fundamental material. The analysis of pair distribution functions (PDF or g(r) is one of the most widely used analysis methods to characterize the atomic scale structure of materials with limited structural coherence. The form of the g(r) function used in MD simulations is given as follows [19–21].

$$g(r) = \frac{\Omega}{N^2}\left\langle \frac{\sum_i n_i(r)}{4\pi r^2 \Delta r} \right\rangle, \qquad (1)$$

where Ω represents the volume of the system and N represents the total number of atoms in the system. n(r) indicates the number of particles in a spherical volume element of thickness Δr. Figure 2 depicts the comparison of liquid g(r) calculated from the TB potential (1850 K) with the experimental g(r) curve (1833 K). EAM and FS potential results are not included here because they have melting point at temperatures higher than the experimental value. It can be seen from the figure that there is a good agreement between the TB-MD simulation results and the experimental g(r). This indicates that the TB potential can successfully explain the structural properties of liquid Fe.

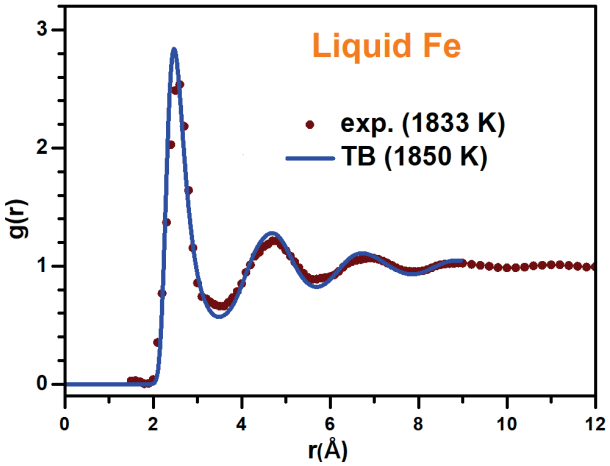

Fig. 2. *Comparison of g(r) calculated from TB-MD simulations at 1850 K with experimental g(r) (1833 K).*

The g(r) calculated using three potentials at different temperatures (500, 1000, 1500, 2000 and 2500 K) are shown in Figure 3. At 500, 1000 and 1500 K, the g(r) calculated from the EAM- and FS-MD simulation are very similar to each other and produce characteristic peaks special to bcc structures. On the other hand, g(r) calculated from the TB-MD simulation produces peaks that are completely different from the others and specific to the hcp/fcc crystal structures. This is an interesting situation and is thought to be due to the TB potential parameters being fitted to the physical properties of γFe at high temperatures [12]. Another reason may be due to the instability of Fe during the heating process, such as bcc-fcc and fcc-bcc phase transitions. In addition, the g(r)'s calculated from the EAM- and TB-MD simulation at 2500 K are similar, but the first peak of g(r) calculated from the FS has a greater width than the others.

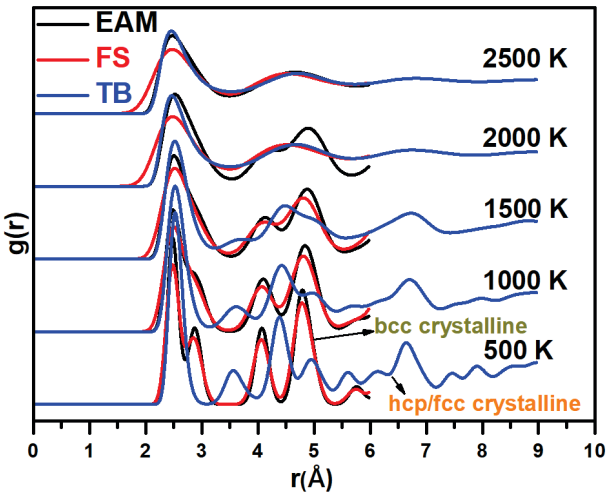

Fig. 3. *g(r) curves calculated at different temperatures from the EAM-, FS- and TB-MD simulations.*

It is of great importance to know what kind of changes occur in the microstructure of the sample examined during the heating or cooling processes [4]. However, g(r) analyzes are insufficient to obtain information about small clusters of atoms in the system. Thus, in our study, Honeycutt-Andersen (HA) bond type index analysis [22, 23], which explains the relationship between bonded pairs and their neighboring atoms, was used in order to analyze the changes in the microstructure of the system in a more detailed and reliable way. In this method, 1421 bonded pairs represent fcc crystal, 1421+1422 bonded pairs hcp crystal, 1441+1661 bonded pairs bcc crystal, 1551 bonded pairs icosahedral and 1431+1541 bonded pairs represent defective icosahedral order, and other uncommon bonded pairs are not given here. The fraction of HA bonded pairs most prevalent in the system during the EAM-MD, FS-MD, and TB-MD simulations is shown in Figure 4 as a function of temperature. The temperature-dependent fraction of HA bonded pairs obtained from the EAM-MD and FS-MD simulation is almost the same. A noticeable change in the fraction of all bonded pairs is observed at the melting point. At this point, while the fraction of 1431 and 1551 bonded pairs, which are more common in liquid and amorphous systems, increase sharply, a significant decrease is observed in the fraction of all other pairs.

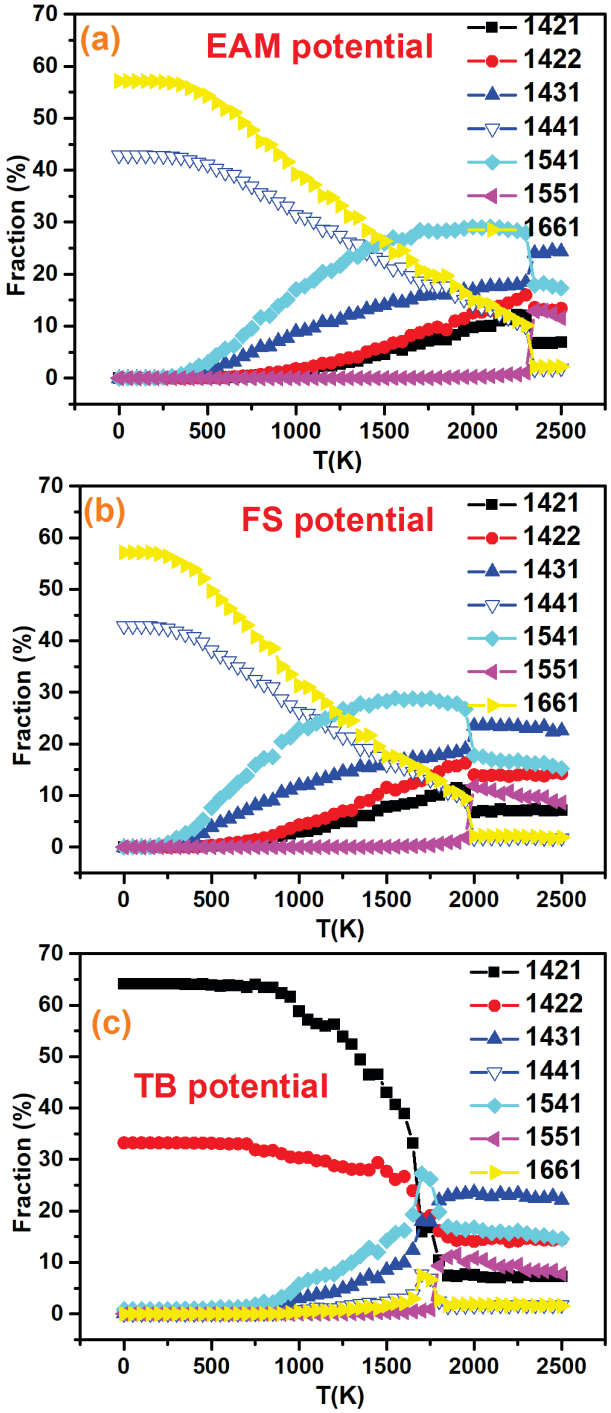

Fig. 4. *Fraction of HA indices most commonly found in the system throughout the (a) EAM-MD, (b) FS-MD, and (c) TB-MD simulations.*

This is a clear indication of the first-order solid-liquid phase transition at these points of the system. Another point is that both potentials preserve the structure of bcc Fe up to its melting point, and in fact, the solid-solid phase transitions observed experimentally during the heating process of Fe are not observed. The situation is much different in the TB-MD simulation results shown in Figure 4(c).

Although the initial system was formed according to the bcc crystal lattice, it is seen that the fraction of 1421 and 1422 bonded pairs around 0 K is around 100% and the fraction of 1441+1611 bonded pairs is around 0%. While there is almost no change in the difference of bonded pairs in the system until around 700 K with increasing temperature, a decrease begins in the fractions of 1421 and 1422 bonded pairs, while an increase in the fraction of 1431 and 1541 bonded pairs begins at the same rate. There is no noticeable increase in the number of 1441 and 1661 bonded pairs representing the bcc structure, but interestingly, a marked jump between 1500 K and 1750 K is observed in the fraction of these pairs and 1541 bonded pairs. This abnormal behavior is also consistent with the V-T and E-T results discussed above. The results for all three potentials at different temperatures (500 K, 1500K and melting temperature) are visualized using the OVITO software [24], and the distributions of bcc, fcc and hcp crystalline atoms in the system are shown in Figure 5, 6 and 7. Supporting the results given in Figure 4, the snapshots obtained from the EAM-MD and FS-M simulation are quite similar to each other. The distribution of atoms with bcc order is always dominant up to the melting point, while the distribution of atoms with the other hcp and fcc crystal order increases slightly with increasing temperature. This is an indication that the EAM and FS potentials maintain the structure of bcc Fe throughout the melting process. Considering the snapshots taken from the TB-MD simulation, it is seen that the atoms in the hcp and fcc crystal arrangement are more at low temperatures, while the distribution of atoms in bcc crystal order is sparse. Interestingly, with increasing temperature, the number of atoms in hcp and fcc crystal order decreases, while the number of atoms in bcc order increases significantly. Especially the visible increase in the number of bcc atoms at 1750 K sheds light on the reason for the abnormal change observed in this temperature range in the other analysis results discussed above. In the light of these findings, in our next study, we will focus on investigating the bcc-hcp/fcc phase transition of Fe under different pressures using the TB potential.

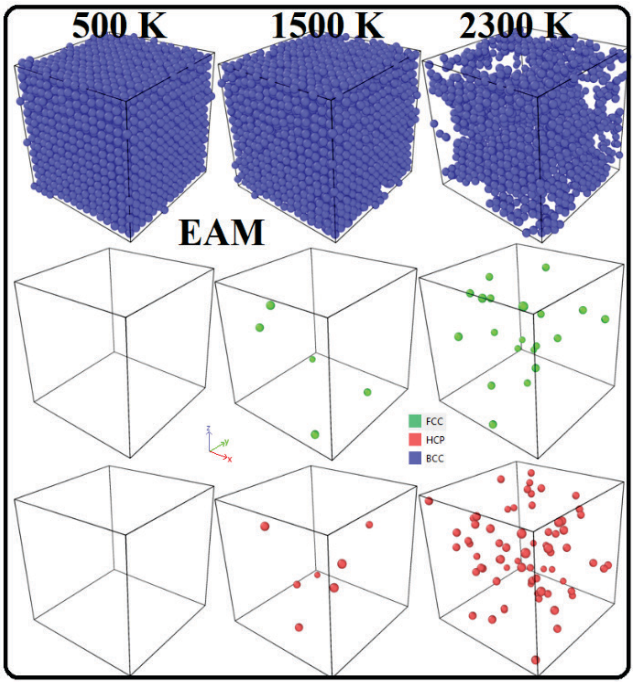

Fig. 5. *Snapshots showing the distribution of atoms arrayed in bcc, hcp, and fcc crystalline patterns at 500 K, 1500 K and 2300 K throughout the EAM-MD simulations.*

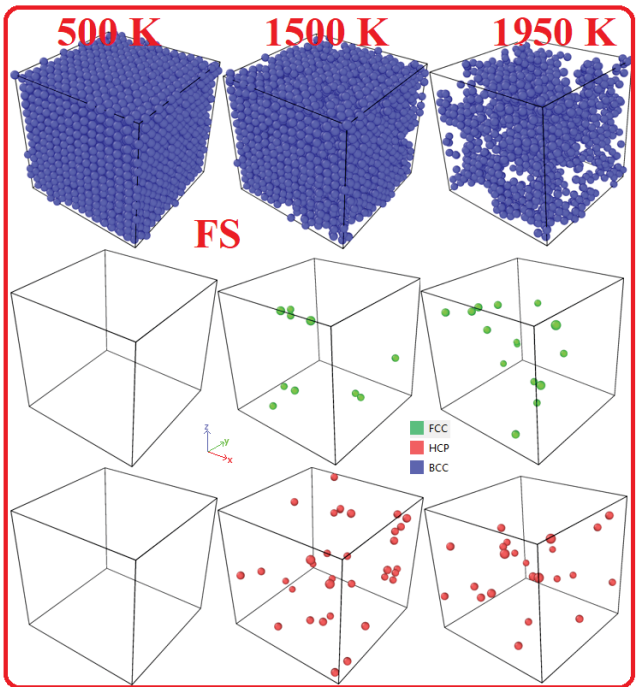

Fig. 6. *Snapshots showing the distribution of atoms arrayed in bcc, hcp, and fcc crystalline patterns at 500 K, 1500 K and 1950 K throughout the FS-MD simulations.*

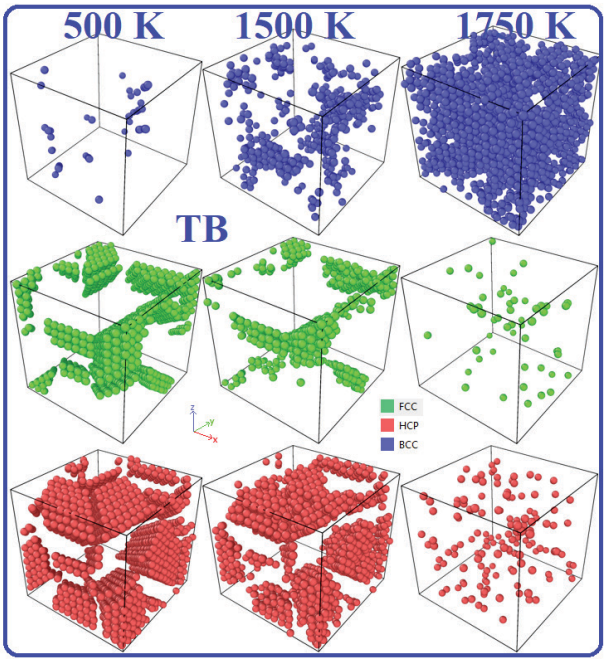

Fig. 7. *Snapshots showing the distribution of atoms arrayed in bcc, hcp, and fcc crystalline patterns at 500 K, 1500 K and 1750 K throughout the TB-MD simulations.*

CONCLUSION

In this study, the melting process of Fe has been investigated by MD simulations using EAM, FS and TB many-body potentials. At low temperatures, it has been observed that the EAM and FS potentials predicted the physical properties of Fe element such as lattice parameter and cohesive energy better than the TB potential. On the other hand, the TB potential predicts the melting point of Fe more accurately than other potentials. The g(r) of liquid Fe calculated from the TB-MD simulations shows good agreement with the experimental g(r) reported in the literature. The EAM and FS potentials maintain the structure of bcc Fe throughout the heating process, while the TB potential predicts the structure of Fe to be stable in the hcp/fcc crystal order even at low temperatures. The results from the EAM-MD and FS-MD simulations are very similar, and their HA analysis results show that 1441 and 1661 bonded pairs are the most dominant pairs during the heating process. In TB-MD simulations, 1421 and 1422 bonded pairs were the most dominant pairs, while a significant increase was observed in 1441, 1661 and 1541 bonded pairs with increasing temperature, especially around the melting point. We believe that our results will provide useful information to

the literature in MD simulation studies of Fe under different conditions.

REFERENCE

[1] Sheng HW, Luo WK, Alamgir FM, et al. Atomic packing and short-to-medium-range order in metallic glasses. Nature 2006; 439: 419–425.

[2] Celtek M, Sengul S. Effects of cooling rate on the atomic structure and glass formation process of Co90Zr10 metallic glass investigated by molecular dynamics simulations. Turkish J Phys 2019; 43: 11–25.

[3] Celtek M. Saf Kalsiyum Elementinin Isıtma Sürecinin Moleküler Dinamik Benzetim Yöntemi ile İncelenmesi. Bitlis Eren Üniversitesi Fen Bilim Derg 2021; 10: 803–815.

[4]Çeltek M, Güder V. Sıvı Vanadyumun Kristalizasyon Sürecine Soğutma Oranı Etkisinin Moleküler Dinamik Benzetim Metodu ile İncelenmesi. Erzincan Üniversitesi Fen Bilim Enstitüsü Derg 2020; 13: 730–745.

[5] Smith W, Forester TR. DL_POLY_2.0: A general-purpose parallel molecular dynamics simulation package. J Mol Graph 1996; 14: 136–141.

[6] Liu C-M, Cheng H-C, Chao C-Y, et al. Phase transformation of high temperature on Fe–Al–Mn–Cr–C alloy. J Alloys Compd 2009; 488: 52–56.

[7] Ou X. Molecular dynamics simulations of fcc-to-bcc transformation in pure iron: a review. Mater Sci Technol 2017; 33: 822–835.

[8] Tateyama S, Shibuta Y, Suzuki T. A molecular dynamics study of the fcc–bcc phase transformation kinetics of iron. Scr Mater 2008; 59: 971–974.

[9] Jeon JB, Lee B-J, Chang YW. Molecular dynamics simulation study of the effect of grain size on the deformation behavior of nanocrystalline body-centered cubic iron. Scr Mater 2011; 64: 494–497.

[10] Finnis MW, Sinclair JE. A simple empirical N -body potential for transition metals. Philos Mag A 1984; 50: 45–55.

[11] Zhou XW, Johnson RA, Wadley HNG. Misfit-energy-increasing dislocations in vapor-deposited CoFe/NiFe multilayers. Phys Rev B 2004; 69: 144113.

[12] Kojima R, Susa M. Second moment approximation of tight-binding potential for γFe applicable up to 1700 K. Sci Technol Adv Mater 2004; 5: 497–502.

[13] Celtek M, Sengul S, Domekeli U, et al. Dynamical and structural properties of metallic liquid and glass Zr48Cu36Ag8Al8 alloy studied by molecular dynamics simulation. J Non Cryst Solids 2021; 566: 120890.

[14] Celtek M. The effect of atomic concentration on the structural evolution of Zr100-xCox alloys during rapid solidification process. J Non Cryst Solids 2019; 513: 84–96.

[15] Cleri F, Rosato V. Tight-binding potentials. Comput Simul Mater Sci 1991; 205: 233–253.

[16] Senturk Dalgic S, Celtek M. Liquid -to-glass transition in bulk glass-forming Cu55-xZr45Agx alloys using molecular dynamic simulations. EPJ Web Conf 2011; 15: 03009.

[17] Celtek M, Sengul S, Domekeli U. Glass formation and structural properties of Zr50Cu50-xAlx bulk metallic glasses investigated by molecular dynamics simulations. Intermetallics 2017; 84: 62–73.

[18] Sengul S, Celtek M, Domekeli U. Molecular dynamics simulations of glass formation and atomic structures in Zr60Cu20Fe20 ternary bulk metallic alloy. Vacuum 2017; 136: 20–27.

[19] Celtek M, Domekeli U, Sengul S, et al. Effects of Ag or Al addition to CuZr-based metallic alloys on glass formation and structural evolution: a molecular dynamics simulation study. Intermetallics 2021; 128: 107023.

[20] Kazanc S, Ahmet Celik F, Ozgen S. The investigation of solid–solid phase transformation at CuAlNi alloy using molecular dynamics simulation. J Phys Chem Solids 2013; 74: 1836–1841.

[21] Sengul S, Guder V. Key factors of deformation mechanism of Cu-Ag alloy. J Non Cryst Solids 2022; 576: 121270.

[22] Honeycutt JD, Andersen HC. Molecular Dynamics Study of Melting and Freezing of Small Lennard- Jones Clusters. J Phys Chem 1987; 91: 4950–4963.

[23] Celik FA, Korkmaz ET. Molecular dynamic investigation of the effect of atomic polyhedrons on crystallization mechanism for Cu-based Cu-Pd and Cu-Pt alloys. J Mol Liq 2020; 314: 113636.

[24] Stukowski A. Visualization and analysis of atomistic simulation data with OVITO-the Open Visualization Tool. Model Simul Mater Sci Eng 2010; 18: 015012.